韓國海洋工學會誌 第11卷 第3號, pp.144~152, 1997. 8

◉ 論 文

On the prediction of global first-year ice loads

Chae-Whan Rim*

(97년 5월 23일 접수)

1년생 빙맥 하중 추정 모델

임 채 환*

Key Words : First-Year Ice Ridge(1년생 빙맥), Ice Loads(빙하중), Keel(수면하부), Sail(수면상부), Consolidated Layer(경화층), Soil Mechanics(토질역학)

초 록

본 논문에서는 1년생 빙맥에 의하여 해양구조물에 작용하는 하중을 추정할 수 있는 모델을 제시하였다. 1년생 빙맥을 수면하부(keel), 수면상부(sail), 경화층(consolidated layer)의 3 부분으로 나누어 각 부분에 의한 하중을 추정할 수 있는 방법을 논의하였다. 수면하부는 얼음조각(ice rubble)이 층으로 쌓여져 형성된 것이므로 수면하부에 의한 하중추정을 할 때 얼음조각을 선형 Mohr Coulomb 재료로 생각하여 토질역학(soil mechanics)의 이론을 사용하였다. 수면상부에 의한 하중도 토질역학 이론을 이용하여 추정하였으며 경화층에 의한 하중은 Korzhavin 식을 이용하여 추정하였다. 제시한 모델을 이용하여 빙맥하중 추정에 미치는 인자들의 영향을 검토하였다.

1. INTRODUCTION

Hydrocarbon resources have been discovered in several Arctic seas where first-year ridges are likely to produce the highest forces on offshore platforms. A study by Shkhinek et al.[1] indicates that there is a significant divergence in methods that are used to calculate design ice loads. Some of these methods have been reviewed by Krankkala & Maattanen.[2] These methods usually consider the ridge keel as a Mohr-Coulomb material and the resistance provided by it is determined using principles of soil mechanics. In particular, efficient use is made of formulas for passive pressure loads on retaining walls.

Soil mechanical approaches lead to formulas that are simple to use and therefore attractive e.g. in a probabilistic ice load determination. However, while using these formulas, the relatively complicated geometry of an ice ridge poses problems with respect to accuracy. Such

* Korea Institute of Machinery and Materials

methods are also difficult in terms of different load limiting mechanisms. The object of this work is to expand the classical soil mechanical approaches for ice ridges by increasing theoretical accuracy and, in addition, to avoid the need for excessive computation.

2. ICE FEATURES CONSIDERED

2.1 ICE RIDGE

Analysis of field data shows that ice ridges may assume several different geometrical forms. Pravdivets et al.[3] propose that the design ice features for offshore structures should include a linear ice ridge as shown in Fig. 1. This type of first-year ice ridge is thought to be a very common ice formation in the pack ice of the Arctic Seas, yielding significant global loads.

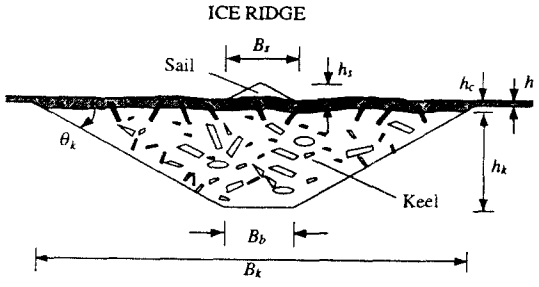

Fig. 1 Cross section and parameters of a linear first-year ice ridge[3].

The cross section of the ridge keel as shown in Fig. 1 is trapezoidal. Lepparanta & Hakala[4] report that this is a common feature for large ice ridges whereas the keels of small ridges tend to be triangular. In subsequent, analysis the geometrical definition of the keel geometry will be simplified by using the keel depth h_k and the inclination angle θ_k as basic parameters and by defining the width of the keel bottom B_b as well as the total ridge width B_k by the equations

$$B_b = \frac{1}{2} h_k \cot \theta_k \quad (1)$$

$$B_k = 2h_k \cot \theta_k + B_b \quad (2)$$

These formulas define the basic geometry of "design ice ridge" to be used in subsequent example calculations.

2.2 FAILURE MODE

The failure mode for the prediction of global load caused by an ice feature is crushing of the consolidated layer against the structure. At the same time, the ridge keel and the rubble accumulation in front of the structure fail along a shear plane. The failure mode is depicted in Fig. 2. The global load arising due to the failure mode is known as "limit-stress" load.

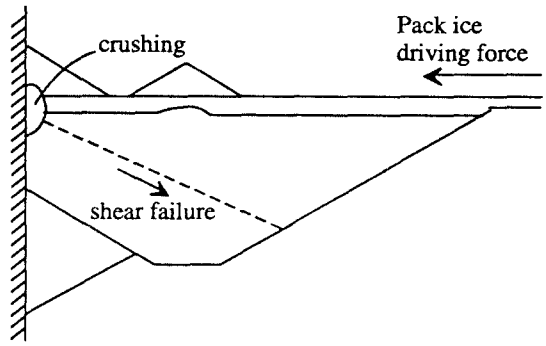

Fig. 2 Ridge failure modes.

3. LOAD ON AN ICE RIDGE

3.1 COMPONENTS OF THE GLOBAL LOAD

The limit-stress load F_{gl} is assumed to be composed of three components as follows:

$$F_{gl} = F_c + F_k + F_s \quad (3)$$

These force components are depicted in Fig. 3. The first component F_c arises from the failure of the consolidated layer and the components F_k

and F_s are termed the keel load component and the rubble (or sail) load component, respectively. In the next, the evaluation of each of these components will be discussed separately.

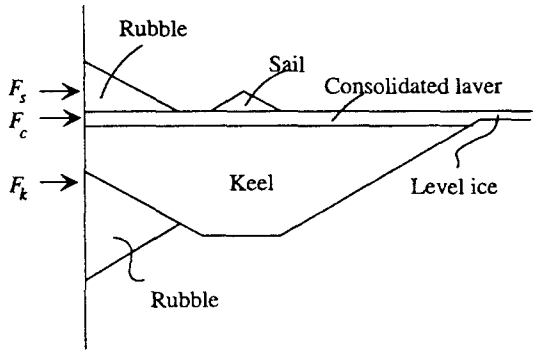

Fig. 3 Components of the global load.

3.2 KEEL LOAD

3.2.1 Simulation of the keel evolution

To determine the load component provided by the ridge keel, how loading conditions develop after initial impact is needed to consider. The keel load component will be determined as a function of the ridge penetration r,

$$F_k = F_k(r) \tag{4}$$

Fig. 4A shows the geometrical condition at a time before the edge O of the ridge profile impacts the structure. At this initial time, an accumulation of ice rubble exists in front of the structure.

The interaction process starts when the edge O of the ridge profile impacts the structure. Fig. 4B shows the keel profile at a later stage when the structure has penetrated into the ridge at a distance r. The coordinate axis xz is fixed at the undeformed position of the structure and the ridge is drifting in the negative direction of the x axis as depicted in Fig. 4B.

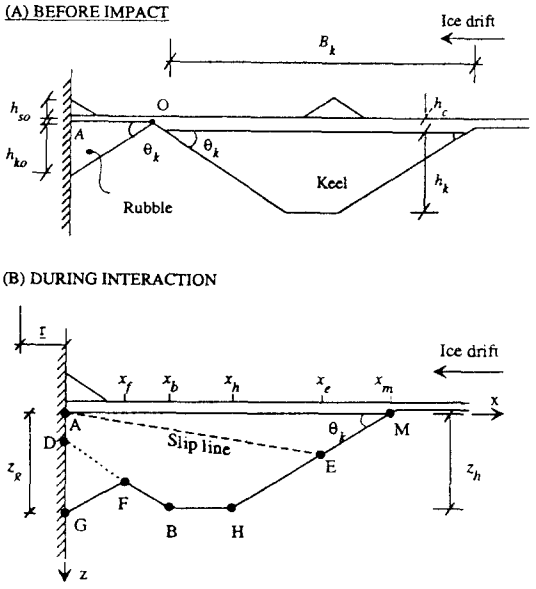

Fig. 4 Conditions before the interaction and during the interaction.

Fig. 5 depicts the basic keel failure mode considered here. The keel experiences several shear failures along slip lines AE that have an inclination ρ_m with the x axis. As will be shown subsequently, the slip angle ρ_m is evaluated by minimizing the keel load component F_k. It will be assumed for the simplicity that the failing block AGFBHE (Fig. 5) undergoes a rigid body displacement relative to the rest of the ridge keel.

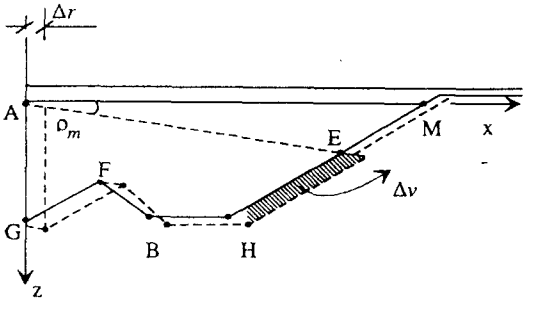

Fig. 5 Shear failure of the keel rubble along a slip plane.

The relative displacements at keel failure are large and secondary failures will occur as indicated in Fig. 5 at the line HE. The keel consists of loose ice blocks. Therefore, the shear failures, together with the secondary failures, result in a sequence of changes in the keel geometry while the structure penetrates the ridge in increments Δr.

3.2.2 Frictional and cohesional keel load components

The present analysis of the keel resistance is based on basic principles of soil mechanics. The ice rubble of the ridge keel will be considered as a linear Mohr-Coulomb material by assuming that plastic yielding will take place when the shear stress reaches the amount

$$|\tau| = c + \sigma_n \tan\phi, \tag{5}$$

where τ is the shear stress at failure on the failure plane, σ_n the normal stress on the failure plane, c is the cohesion and ϕ the internal friction angel.

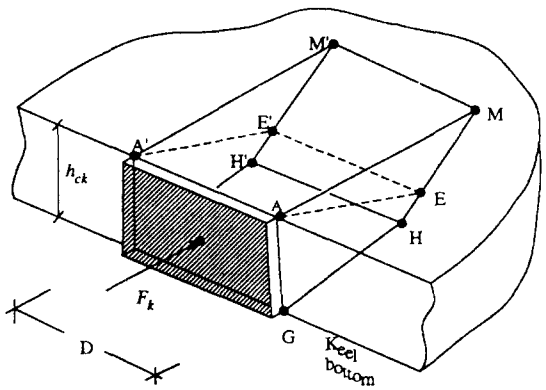

Fig. 6 Assumed failure mechanism with an inclined and two vertical slip planes.

Fig. 6 depicts the ridge keel that is pressed by the force F_k through a rigid wall. It is assumed that keel failure occurs along an inclined failure surface AEE'A' and the two vertical planes AGHE and A'G'H'E' as shown in Fig. 6. The frictional and cohesional forces that act on these slip planes and resist the acting contact force F_k are separately examined in the next.

Frictional resistance at the inclined slip plane

Fig. 7 depicts the cross section of the ridge keel at the failure condition. The inclination angle of the slip plane is defined by the parameter ρ. The forces Q, S, and $R_{1\phi}$ shown in this figure are now used to evaluate the keel load component $P_{1\phi}$ that arises due to the frictional resistance at the slip plane AEE'A'.

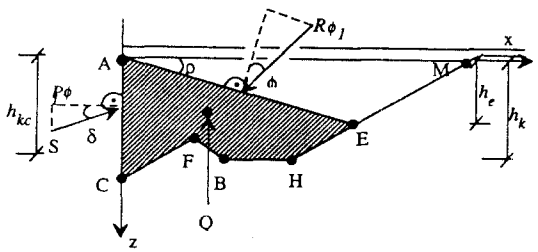

Fig. 7 Forces acting on the failing rubble volume.

It is noted that some frictional forces act between the structure and the ice rubble. These forces are defined by the friction angle δ and can combined, together with the horizontal force $P_{1\phi}$, into a force resultant

$$S = P_{1\phi} \cos^{-1}(\delta + \alpha_s) \tag{6}$$

The angle α_s is the inclination of the structure wall and is defined as positive for walls that force a drifting ice sheet upwards.

The buoyancy force Q is evaluated as

$$Q = \gamma_k DA \tag{7}$$

where D is the structure width, A is the area of the cross section AGFBHE, and γ_k is the rubble buoyancy given by

$$\gamma_k = (1-n)(\rho_w - \rho_i)g \tag{8}$$

Here, n is the porosity of the keel rubble, g is the acceleration due to gravity and ρ_w, ρ_i are water and ice densities, respectively.

After these preparations the following two equations of equilibrium are driven, the first in the direction of the slip plane and the second perpendicular to this direction.

$$S\cos(\delta+\rho+\alpha_s) - R_{1\phi}\sin\phi - Q\sin\rho = 0 \tag{9a}$$

$$-S\sin(\delta+\rho+\alpha_s) + R_{1\phi}\cos\phi - Q\cos\rho = 0 \tag{9b}$$

Solving these equations for S and substituting Eq. (6), we find

$$P_{1\phi} = Q\frac{\sin(\rho+\phi)}{\cos(\delta+\rho+\phi+\alpha_s)}\cos(\delta+\alpha_s) \tag{10a}$$

A restriction was imposed on applying this equation

$$\delta+\rho+\phi+\alpha_s < \frac{\pi}{2} \tag{10b}$$

to prevent the occurrence of numerical instability and negative values for $P_{1\phi}$.

Cohesional resistance at the inclined slip plane

The resistance provided by the rubble cohesion at the slip plane is calculated simply by multiplying the keel cohesion by the area of the slip plane. However, it can be anticipated that keel cohesion varies with the depth coordinate z. An effective keel cohesion c_{eff} that varies with the slip angle as shown in Fig. 8 is given by

$$c_{eff} = \begin{cases} c_1 + \dfrac{c_2 - c_1}{\rho_2}\rho, & \text{for } 0 \le \rho \le \rho_2 \\ c_2, & \text{for } \rho > \rho_2 \end{cases} \tag{11}$$

In the subsequent sample calculations it is assumed that $\rho_2 = 30°$.

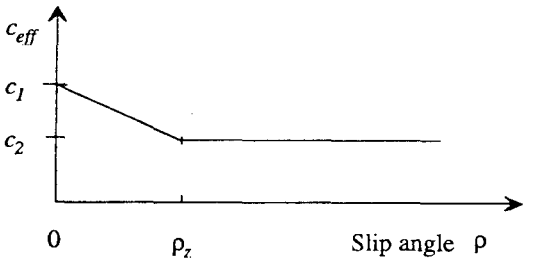

Fig. 8 Effective keel cohesion as a function of the slip angle.

With the definition given by Eq. (11), the cohesional resistance provided by the inclined slip plane can be evaluated as

$$P_{1c} = c_{eff}Dh_e\cos\rho/\sin\rho \tag{12}$$

Frictional resistance at the vertical slip planes

The resultant of the normal pressures acting on the vertical slip surface AGFBHE which is shown in Figs. 6 and 7 is defined by

$$R_{2\phi} = \int_A \gamma_k z dA \tag{13}$$

A closed form solution for this integral is very extensive and the cross section will therefore be simplified. The broken lower boundary line GFBH of the keel rubble is replaced by an equivalent straight line, CH. The z-coordinate of the auxiliary point C is given by

$$z_c = \frac{1}{2}(z_g + z_f) \tag{14}$$

With this simplification Eq (14) can be evaluated by

$$R_{2\phi} = \frac{\gamma_k}{6}[x_h z_c(z_c+z_h) + (x_e - x_h)z_c(z_h+z_e) + x_e z_h^2 - x_e^3\tan^2\rho] \tag{15a}$$

Considering that this normal force is acting on two vertical slip planes, the frictional resistance provided by these planes can be evaluated as

$$P_{2\phi} = 2R_{2\phi}\tan\phi\cos\rho \tag{15b}$$

Cohesional resistance at the vertical slip planes

Cohesional force P_{2c} acting at the vertical slip plane is given by

$$P_{2c} = 2c_2 A \cos\rho \tag{16}$$

3.2.3 Total resistance provided by the keel

The Eqs. (10), (12), (15) and (16) for the various frictional and cohesional force components represent peak values for each of these forces. The formulas were derived separately because peak values may not occur simultaneously. To increase the accuracy of estimations, the frictional and cohesional keel load components are combined into the total keel load component as a root of the sum of squares:

$$F_k = \sqrt{(P_{1\phi} + P_{2\phi})^2 + (P_{1c} + P_{2c})^2} \tag{17}$$

3.3 RUBBLE PILE LOAD

The sail of the actual ice ridge is not relevant while calculating the global load because the maximum keel load component occurs before the ridge sail meets the structure. However, the effects of the rubble pile that develops in front of the structure will be considered.

The frictional and cohesional loading components are given by

$$F_{s\phi} = \frac{1}{2}\gamma_s D h_{sr}^2 K_p \tag{18}$$

$$F_{sc} = 2Dch_{sr}\sqrt{K_p} \tag{19}$$

where γ_s is the specific weight of the rubble pile given by

$$\gamma_s = (1 - n_r)\rho_i g \tag{20}$$

and n_r is the rubble porosity. It is assumed that the porosity of the rubble is the same as for the keel.

The coefficient K_p in Eq. (18) is the passive pressure coefficient given in the form,

$$K_p = \sin^2(\alpha - \phi)/(\sin^2\alpha \sin(\alpha + \delta) \left[1 - \sqrt{\frac{\sin(\phi + \delta)\sin(\phi + \beta)}{\sin(\alpha + \delta)\sin(\alpha + \beta)}}\right]^2) \tag{21}$$

The load component due to the rubble pile is small compared with the keel load component. Therefore, the contribution of the vertical slip planes that were considered for the keel can be ignored. Corresponding to the keel load component, the total resistance provided by the sail is evaluated as

$$F_s = \sqrt{F_{s\phi}^2 + F_{sc}^2} \tag{22}$$

3.4 CONSOLIDATED LAYER LOAD

Any new techniques will not be developed here to evaluate loads caused by level ice or the consolidated portion of the ridge. Instead, it is assumed that the resistance provided by the consolidated layer is given by the simple formula

$$F_c = p_{cr} h_c D \tag{23}$$

where h_c is the thickness of the rafted and consolidated layer, D is the width of the structure and p_{cr} is the nominal ice crushing pressure on the total ice-structure interface. Any available method to evaluate p_{cr} can be applied and p_{cr} is used as an input parameter in the computer program associated to the present method.

4. PARAMETRIC STUDIES

A computer program was written to solve the equations developed in sections 1 through 3. This program was used to study some basic features of the model and the various force components. Ridge action was examined against a gravity-based, rigid platform. The assumed

ridge geometry and the ridge strength characteristics are given in Table 1.

To consider the consequences of increased the apparent cohesion in the upper portion of the keel, the ratio between the two cohesion parameters was varied in the range of c_1/c_2 = 1-20. The results of this parametric study are shown in Fig. 9 and in Table 2.

Table 1 Basic parameters of sample calculations.

Structure		Ridge geometry		Ridge characteristics	
D (m)	100	h (m)	1.5	ϕ	30 - 55
α_s (deg)	0	h_c (m)	3.0	c_2 (kPa)	3
δ (deg)	0 or 10	h_k (m)	20	c_1/c_2	1- 20
		h_{k0} (m)	8	n	0.25
		θ_k (deg)	30	P_{c1} (MPa)	0.65
		B_k (m)	86.6	P_{rh} (MPa)	0.40
		L (m)	500	γ_k (N/m^3)	750

In all three cases studied, the slip angle was large at the beginning of the interaction. If the cohesion was assumed to be uniform within the keel (c_1/c_2 = 1) the slip angle decreased to zero at a larger ridge penetration. This type of failure mode is sometimes termed as "plug failure". Due to the assumed "shear keys" between the consolidated layer and the ridge keel, the slip angle ρ grows with the ratio c_1/c_2. Correspondingly, the maximum keel load component grows significantly.

Table 2 Influence of the cohesion ratio on the condition of maximum keel resistance. Friction coefficients: δ=10 degrees and ϕ=45 degrees.

Cohesion ratio c_1/c_2	Condition of maximum keel resistance		
	F_k (MN)	r (m)	ρ_m (deg)
1	110	15	8.4
10	150	20	17.1
20	182	21	20.6

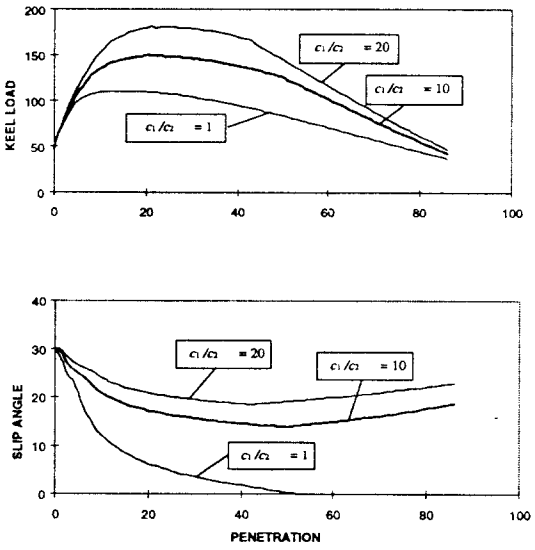

Fig. 9 Influence of the layered keel structure. Friction angles ϕ=45 deg. and ϕ=10 deg.

The maximum value of the keel load component F_k as a function of the frictional parameters δ and ϕ, while keeping the other parameters constant is examined. The friction angle of the structure surface δ was varied from 0 to 10 degrees. ϕ was varied from 30 to 55 degrees. The ratio between the cohesional parameters was selected as c_1/c_2 = 10. The results are given in Fig. 10 and in Table 3.

Table 3 Influence of the friction angles δ and ϕ on the maximum keel load component. Cohesion ratio c_1/c_2 = 10.

δ (deg.)	ϕ (deg.)	Condition of maximum keel load component		
		F_k (MN)	r (m)	ρ_m (deg)
0	30	74	28	27.6
10	30	90	27	23.5
10	45	150	20	17.1
10	45	220	15	11.6

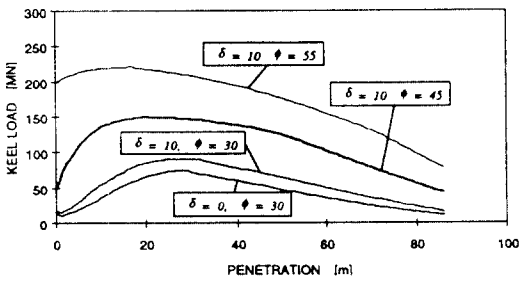

Fig. 10 Influence of the variations in the friction angles δ and φ. Ratio of the cohesion parameters c_1/c_2 = 10.

This simulation shows that the slip angle corresponding the maximum keel load decreases with an increase in the friction coefficients. An increase in the friction angle δ at the structure surface from zero to 10 degrees resulted in an increase in the keel load F_k from 74 MN to 90 MN. The keel load further increased to 150 MN, when the internal friction angle of the keel was changed from 30 degrees to 45 degrees. A final change of φ to 55 degrees yielded a maximum keel load of 220 MN. This shows that the uncertainty in the internal friction coefficient has a significant influence on the keel load component and also on global load estimates.

A further parametric study was done to determine the significance of the different resistance components arising in the inclined and horizontal slip planes. The result is shown in Fig. 11 and in Table 4 for a specific combination of strength characteristics. It is clear that the resistance provided by the inclined slip plane is dominant.

Table 4 Components of the maximum keel load F_k = 150 MN that was found for δ = 10 deg., φ = 45 deg. and c_1/c_2 = 10.

F_k (MN)	Components (MN)			
	$P_{1\phi}$	P_{1c}	$P_{2\phi}$	P_{1c}
150	119	70	12	3

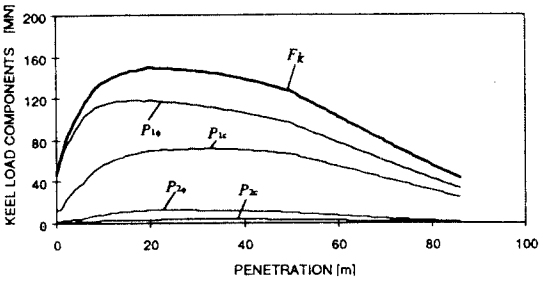

Fig. 11. Components of the keel resistance. Friction angles φ = 45 deg. and δ = 10 deg. Ratio of the cohesion parameters c_1/c_2 = 10.

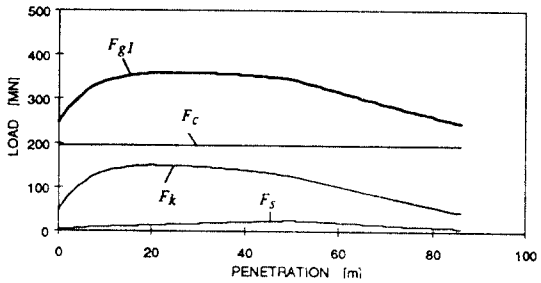

Fig. 12 The components F_c, F_k and F_s of the limit-stress load F_{gl}. Friction angles φ = 45 deg. and δ = 10 deg. Ratio of the cohesion parameters c_1/c_2 = 10.

The forces arising from the two vertical slip planes shown in Fig. 6 contribute to less than 10 % the keel load.

Fig. 12 shows the composition of the limit-stress load F_{gl} as the sum of the forces arising from the consolidated layer (F_c), the ridge keel (F_k) and from the rubble pile (F_s). The maximum of F_{gl} is 359 MN. The contributions of the components F_c, F_k and F_s to the maximum value are 54%, 41% and 5%, respectively. The nominal crushing pressure of 0.65 Mpa was used to calculate the load component F_c. It appears that the consolidated layer provides the highest load contribution in the case of vertical-faced structures. For the case of an inclined structure,

the component F_c will decrease and the keel load F_k component will increase as shown by Eq. (10). Therefore, the keel load component can become dominant in the case of an inclined structure.

5. SUMMARY

A model and associated computer program was developed for a deterministic prediction of global first-year ice loads on offshore structures. The load caused by a ridge consists of load components arising from a consolidated layer, a rubble pile that develops in front of the structure and of the ridge keel. The ridge keel is considered as a layered accumulation of ice rubble, below the consolidated layer. The uppermost layer of the ridge keel can have a high apparent cohesion strength, due to ice blocks that are partially frozen into the consolidated layer.

A soil mechanical approach is used to simulate the changes in the keel profile when a structure penetrates the ridge. Both vertical and inclined structures can be considered by the present model.

A parametric study was made to determine how some of the uncertainties of the input parameters influence the global load evaluation. Therefore, it should be appreciated that the example calculations shown above do not represent actual ice load predictions for the example structure considered. It was found that the present lack of knowledge about the internal friction angle of the ridge keel represents a major source of uncertainty in ice load prediction. The computations also showed that the layered structure of the ridge keel may influence the keel load component considerably. The frictional resistance that develops at the rubble/structure contact area causes an increase in the ice load. The inclination of the structure has the same effect if the ice wall forces the ice rubble upwards during ridge penetration.

ACKNOWLEDGMENTS

This work is a part of a joint research project between Korea Institute of Machinery and Materials, and Technical Research Center of Finland. It was funded by the Ministry of Science and Technology of Korea. The author wishes to acknowledge this support. Numerous discussions with Dr. Tuomo Kärnä are appreciated.

REFERENCES

1) Shkhinek, K., Blanchet, D., Croasdale, K., Matskevitch, D. & Bhat, S., "Comparison of the Russian and foreign codes and methods for global load estimations," Proc. 13th International Conference on Offshore Mechanics and Arctic Engineering, (OMAE-94), Vol. IV, pp. 75-82, 1994

2) Krankkala, T. & Määttänen, M., "Methods for determining ice forces due to first- and multi-year ridges," Proc. 7th IAHR Ice Symposium (IAHR-84), Hamburg, pp. 263-287, 1984

3) Pravdivets, J., Rogachko, S., Evdokimov, G., Melnikov, G., & Kärnä, T., "Choice of Offshore Structures for Arctic Regions," VTT building Technology Report RTE38-IR-4, 1997

4) Leppäranta, M. & Hakala, R., "The structure and strength of first-year ice ridges in the Baltic Sea," Cold Regions Science and Technology, 20(1992), pp. 295-311, 1992